Chemistry
A European
Journal

Chemistry Europe
European Chemical Societies Publishing

## Accepted Article

**Title:** Implementation of the Hard-Soft Acid-Base Principle for the Direct Synthesis of Bimetallic Zirconium-Nickel and Hafnium-Nickel Metal-Organic Frameworks with a Polar Pore Environment

**Authors:** Pantelis Trikalitis, Konstantinos G. Froudas, and Giasemi K. Angeli



**To be cited as:** *Chem. Eur. J.* **2025**, e202501049

**Link to VoR:** https://doi.org/10.1002/chem.202501049

WILEY VCH

10.1002/chem.202501049





# Implementation of the Hard-Soft Acid-Base Principle for the Direct Synthesis of Bimetallic Zirconium-Nickel and Hafnium-Nickel Metal-Organic Frameworks with a Polar Pore Environment

Konstantinos G. Froudas,[a] Giasemi K. Angeli [a,b] and Pantelis N. Trikalitis*[a]

[a] Department of Chemistry, University of Crete, Voutes 70013 Heraklion, Greece
[b] Theoretical and Physical Chemistry Institute, National Hellenic Research Foundation, 48 Vassileos Constantinou Avenue, Athens, 11635 Greece

## Abstract

An important direction in MOFs is the development of materials with well-defined and ordered heterogeneity towards novel functionalities and control of important properties at the atomic scale. A great approach is the designed synthesis of mixed metal MOFs (M'MOFs) made of different building units, based on distinct metal cations. However, their in-situ formation and co-assembly into an extended crystalline framework present great challenges due to the different kinetic and thermodynamic parameters. We report the successful synthesis of two isostructural, bimetallic Zr-Ni and Hf-Ni M'MOFs following the hard and soft acid and base (HSAB) principle. Single crystal X-ray diffraction analysis revealed the formation of a 3D structure that features an *in-situ* formed $[Ni(HPyC)_4Cl_2]^{4-}$ 4-c non-planar metallo-ligand, that bridges 8-c $Zr(Hf)_6$-clusters. The resulting (4, 8)-c **scu** type framework shows polygonal 1D channels, with a largest pore diameter of approximately 9 Å, decorated by $Cl^-$ anions. This polar pore environment was found fully accessible and both materials were investigated for Xe/Kr and $CO_2/CH_4$ separation. The results are very promising showing that the IAST selectivity calculated for a 20:80 Xe/Kr molar mixture is 8.2 and 7.1 at 298K for the Zr_Ni-**scu**-MOF-1 and Hf_Ni-**scu**-MOF-1, respectively, which is comparable to some of the best performing materials.

## INTRODUCTION

Possessing the advantages of permanent and tunable porosity, Metal-Organic Frameworks (MOFs) represent an important class of crystalline solids with impressive capabilities that can address long-standing energy and environmental sustainability challenges.[1-7] The high degree of modularity that these hybrid materials inherently display, originating from the properties of the organic and inorganic building components, coupled with high porosities, enables the construction of materials with fine-tuned chemical compositions and structural characteristics for the targeted application, aided by the reticular chemistry approach.[8-16]

There is a continuously growing need for new generation MOFs with enhanced properties. In this essence, more complex, but still ordered structures composed of two or more metals have emerged.[17-19] The heterogeneity of such multifunctional solids promotes synergistic

10.1002/chem.202501049





effects, which are reflected in a superior performance in a number of key applications, including gas storage and separation[20-22], heterogeneous catalysis[23-25] and sensing, among other. In particular, within mixed metal MOFs (M'MOFs), those consisting of different types of inorganic building units have attracted great attention as distinct, adsorption and/or catalytically rich sites are immobilized in the backbone of the MOF in a periodic way.[26-29] The use of metallo-ligands in constructing M'MOFs has been successfully utilized by our group and others, as for example in the synthesis of $Pd^{2+}$-incorporated $Cu^{2+}$-**nbo** and $M^{3+}$-**soc** (M: Fe, In) MOFs showing exceptional $CO_2$ uptake due to the synergistic action of unsaturated acidic $Cu^{2+}$ and basic $Pd^{2+}$ sites, as well as important catalytic properties.[30-32] Similarly, pre-constructed metal-organic molecular complexes with uncoordinated terminal moieties can be introduced in MOF synthesis as well-defined building blocks, whose rational assembly with a second metal ion directs the emergence of a crystalline framework.[33-37] Nevertheless, there is a finite number of such building units with available donor groups who can be isolated, while their solubility and/or structural integrity under the reaction conditions is an often obstacle.

On the other hand, the one-pot generation of M'MOFs structures without a preformed metallo-ligand remains a challenge, as the deviation in reaction kinetics between the different metal cations often precludes their co-incorporation in the same framework structure. Along the above lines, mixed phases are frequently encountered, while the reported examples of M'MOFs with two distinct secondary building units (SBUs) are usually restricted to either metal ions of comparable valence and ionic radius or these are based on bifunctional organic ligands that promote the formation of different SBUs and their subsequent reticulation into a porous framework.[28-29] In a noticeable example, Rosi and co-workers have reported the synthesis of new families of heterobimetallic MOFs with programmable topologies using the bifunctional isonicotinate linker and its derivatives, which can coordinatively distinguish between early and late transition metals, and isolated M'MOFs with **fcu**, **ftw** and **pfm** topologies based on the combination of hexanuclear $M_6$-clusters (M: $Zr^{4+}$, $Hf^{4+}$, $Dy^{3+}$) and different transition metal cations.[38]

In the present work, we report the one-pot rational construction of two bimetallic Zr-Ni and Hf-Ni M'MOFs by the deliberate practice of hard and soft acid and base (HSAB) principle. In particular, a bifunctional ligand, namely 1H-pyrazole-4-carboxylic acid ($H_2PyC$) was purposely selected as it comprises of a hard carboxylate and a soft pyrazolate coordinating group and reasonably we targeted the preferential binding of the former to a hard Lewis acid ($Zr^{4+}$ or $Hf^{4+}$) and the latter to a soft Lewis acid ($Ni^{2+}$). Markedly, the resultant 3D framework features an *in-situ* formed octahedral $Ni^{2+}$ metal-organic complex, serving as a tetratopic metallo-ligand which drives the formation of an eight-connected (8-c) hexanuclear $[Zr_6O_4(OH)_4]^{12+}$ (or $[Hf_6O_4(OH)_4]^{12+}$) cluster and the subsequent generation of two novel isostructural bimetallic Zr-Ni and Hf-Ni M'MOFs with **scu** topology, denoted as M_Ni-**scu**-MOF-1 (M: $Zr^{4+}$, $Hf^{4+}$). While this work was in preparation, an isostructural Zr-Co-based analogue was reported.[39] Notably, the Zr(Hf)-Ni

combination is missing in the heterometallic MOF literature, excluding MOFs based on metalated porphyrins as in these cases the presence of the transition metal cations is not essential for the formation of the framework.[40] Therefore, our work represents the first examples of bimetallic MOFs based on distinct $Zr^{4+}$/$Hf^{4+}$ and $Ni^{2+}$-based building units, generated through one-pot synthesis reactions and opens new possibilities toward the systematic exploration of multifunctional polymetallic MOFs.

The reported materials show permanent and fully accessible porosity, while the polar pore environment, arising from different functionalities including coordinating chloride anions and non-coordinating NH-sites on the metallo-ligand, prompted us to examine its performance in Xe/Kr as well as $CO_2/CH_4$ separation. In the case of Xe/Kr, the results are very promising showing that the IAST selectivity calculated for a 20:80 molar mixture is 8.2 and 7.1 at 298K for the Zr_Ni-**scu**-MOF-1 and Hf_Ni-**scu**-MOF-1, respectively, which is higher compared to reported MOFs with a similar pore size and comparable to some of the best performing materials.

## RESULTS AND DISCUSSION

The solvothermal reaction between $ZrCl_4$, $Ni(NO_3)_2{\cdot}6H_2O$ and 1H-pyrazole-4-carboxylic acid ($H_2PyC$) in N,N'-dimethylformamide (DMF) at 120 $^oC$ for 2 days in the presence of trifluoroacetic acid (TFA) acting as modulator, afforded high quality rod shaped single crystals. Single crystal X-ray diffraction (SCXRD) studies (see SI) show that Zr_Ni-**scu**-MOF-1 crystallizes in the orthorhombic space group *C*mmm with lattice parameters a=21.706(3) Å, b=21.965(3) Å, c=12.3774(17) Å and V=5901.2(13) $Å^3$. The structure is composed of 8-connected $[Zr_6(\mu_3\text{-}OH)_4(\mu_3\text{-}O)_4]^{12+}$ carboxylate-based clusters (Figure 1a) and 4-connected $[Ni(HPyC)_4Cl_2]^{4-}$ pyrazole-based metallo-ligands (Figure 1b), which apparently are formed *in situ*. The assembly of the aforementioned building units results in a 3-dimensional (4,8)-connected framework that displays the **scu**-a topology (Figure 1c, d). Concerning the *in situ* formed metallo-ligand, an octahedral complex of $Ni^{2+}$ serves as a well-defined tetratopic, 4-c building unit. In this complex, the axial positions of $Ni^{2+}$ are occupied by coordinated $Cl^-$ anions, present in MOF's synthesis from the $Zr^{4+}$ precursor, while the equatorial positions are occupied by four N-atoms, from four different $[HPyC]^-$ molecules, which bind in a monodentate fashion to the metal center. Accordingly, the metallo-ligand has four available carboxylate groups which are found coordinated to the $Zr_6$-cluster. Notably, the particular coordinating arrangement of the pyrazole on $Ni^{2+}$ results not in a planar 4-c metallo-ligand but rather, a three-dimensional (3D) metallo-organic building block (Figure 1b). In particular, due to the monodentate coordination mode of the pyrazole group, pairs of non-coordinating NH-sites are placed above and below the equatorial plane of the $Ni^{2+}$ octahedral complex. This in turn results in a similar up and down arrangement of the carboxylate groups, making the overall metallo-ligand a 3D, 4-c building unit. It is important to note that the 3D conformation of the metallo-ligand is in contrast to the planar arrangement

10.1002/chem.202501049

of 4-c ligands used to construct MOFs with **scu**-a topology, based on $Zr_6$-, $Hf_6$- and $Ce_6$(IV)-clusters (Figure S3).[41-44]

The uncommon non-planar metallo-ligand impacts the pore geometry and functionality in Zr_Ni-**scu**-MOF-1. Accordingly, the porous framework encloses polygonal 1D channels running along the *c* axis, with a largest pore diameter of approximately 9 Å, decorated by $Cl^-$ anions (Figure 1c). These 1D channels are interconnected via smaller windows of approximately 5 Å looking down the [110] crystallographic direction (Figure S2). This is also confirmed by the void space analysis of Zr_Ni-**scu**-MOF-1 using the Pore Analyser tool available in Mercury[45], where the maximum pore diameter was found to be 9.2 Å (Table S3). As we report below, this pore network was found to be accessible and studied by detailed gas sorption experiments.

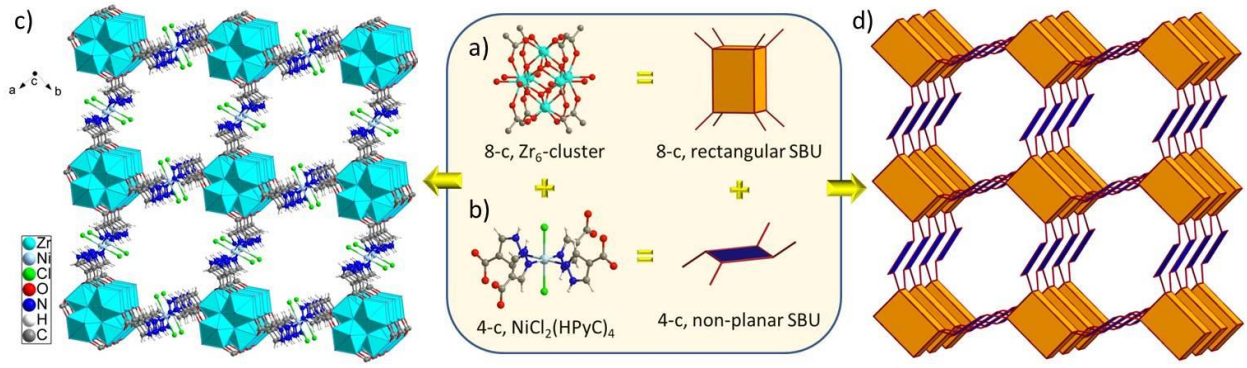


**Figure 1.** The combination of 8-c hexanuclear $Zr_6(\mu_3\text{-}O)_4(\mu_3\text{-}OH)_4(H_2O)_4(OH)_4(\text{-}COO)_8$ clusters (a), acting as an 8-c rectangular SBUs, with the *in situ* formed $Ni(HPyC)_4Cl_2$ metallo-ligands serving as 3D, 4-c non-planar SBUs (b), results in the construction of Zr_Ni-**scu**-MOF-1 (c), displaying the augmented **scu**-a net (d).

Notably, as revealed from the crystal structure of Zr_Ni-**scu**-MOF-1 and supported by infrared spectroscopy measurements, the pyrazole rings remain protonated (Figure S5). The N…Cl distance of 3.06 Å between the non-coordinating NH groups and the Cl atoms on the axial positions, is shorter than the sum of the corresponding Van der Waals radius (3.3 Å), indicating the formation of intramolecular hydrogen bonds, which presumably help the formation and stabilization of the metallo-ligand (Figure S4). Although, this kind of $M^{2+}$ tetrakis-pyrazole (M: $Cu^{2+}$, $Co^{2+}$, $Mn^{2+}$, $Ni^{2+}$) molecular complexes are known in coordination chemistry,[46-47] its systematic generation under MOFs synthesis conditions is challenging due to the well-known partial decomposition of DMF at elevated temperatures, generating dimethylamine that could deprotonate the pyrazole ring. This particular role of DMF has been successfully utilized towards the formation of crystalline pyrazolate-based MOFs.[48-49] In our work, the acidic reaction conditions originating from the presence of trifluoroacetic acid (TFA) acting as modulator for the formation highly crystalline product, apparently prohibits the deprotonation of the pyrazole group and drives the in-situ formation of the non-planar, 4-c metallo-ligand, described above.

10.1002/chem.202501049





Notably, the choice and the amount of TFA in the reaction mixture were found to be crucial (see Table S1). For example, the use of benzoic acid instead of TFA, which is frequently used in synthesis of Zr-based MOFs resulted in amorphous solids. Apparently, the highly acidic TFA (pKa 0.23) as compared to the benzoic acid (pKa 4.2) controls efficiently the reaction kinetics and promotes the formation of crystalline Zr_Ni-**scu**-MOF-1. Interestingly, under the same reaction conditions, the cobalt analogue is not formed. However, this material, denoted as FDM-182, was synthesized without any modulator, by performing the reaction at 65 $^{o}$C in DMF, as reported recently.[39]

The overall charge-balanced chemical formula of Zr_Ni-**scu**-MOF-1 is $Zr_6(\mu_3\text{-}OH)_4(\mu_3\text{-}O)_4(OH)_4(H_2O)_4[Ni(HPyC)_4Cl_2]_2$. The phase purity of the crystalline material was confirmed by the excellent match between the experimental powder X-ray diffraction (PXRD) pattern and that calculated from the single-crystal structure (Figure S6). Furthermore, the Zr:Ni:Cl atomic ratio obtained from energy dispersive spectroscopy (EDS) measurements, executed in a scanning electron microscope (SEM), is 3:0.94:1.90, which is in very good agreement with the expected value of 3:1:2 based on the chemical formula (Figure S10).

The Hf-analogue, Hf_Ni-**scu**-MOF-1, was synthesized by slightly modified reaction conditions and confirmed to be isostructural to Zr_Ni-**scu**-MOF-1 by PXRD measurements (Figure S6). Both materials retain their structural integrity after soaked in various organic solvents as studied by PXRD (Figures S7 and S8). Thermogravimetric analysis (TGA) of the as-synthesized materials revealed that, following the initial solvent loss, a broad weight-loss step occurs between 250–450 °C, corresponding to framework decomposition (Figure S11). This behavior is consistent with the reported TGA curve of the cobalt analogue FDM-182, indicating that these materials share similar thermal stability and decomposition mechanisms. Pore activation was straightforward using acetonitrile as a volatile solvent to exchange the DMF molecules followed by overnight drying under high vacuum at room temperature. Prior to the evacuation, the complete removal of DMF molecules was confirmed by $^{1}$H NMR spectroscopy on acid digested samples (Figures S41 and S42). The permanent porosity of both MOFs was confirmed by recording Ar sorption measurements at 87 K (Figure 2a), illustrating fully reversible type-I isotherms, characteristic of microporous materials. In particular, Zr_Ni-**scu**-MOF-1 has a Brunauer-Emmett-Teller (BET) surface area of 927 $m^2\ g^{-1}$ (Figure S12) and a total pore volume of 0.38 $cm^3\ g^{-1}$ at 0.99 $p/p_0$ (Ar total uptake, 297.3 $cm^3\ g^{-1}$), which is lower compared to the expected value from the single crystal structure (0.56 $cm^3\ g^{-1}$). The corresponding values for Hf_Ni-**scu**-MOF-1 are 632 $m^2\ g^{-1}$ (Figure S12) and 0.28 $cm^3\ g^{-1}$, respectively. The observed lower gravimetric values are consistent with the heavier framework of the Hf analogue. Considering the crystallographic density of Zr_Ni-scu-MOF-1 (1.098 g $cm^{-3}$) and calculating the corresponding value for Hf_Ni-scu-MOF-1 (1.393 g $cm^{-3}$), the obtained volumetric BET surface area is 1017.9 $m^2\ cm^{-3}$ and 880.2 $m^2\ cm^{-3}$ respectively, indicating a small difference in porosity between the two solids.

10.1002/chem.202501049





It is noted that the isostructural Zr_Co analogue, FDM-182, shows a slightly lower BET area of 862 $m^2\ g^{-1}$ and an almost identical Ar total uptake at 87 K (the plateau at close to 0.99 $p/p_0$ is ~300 $cm^3\ g^{-1}$), suggesting a very similar total pore volume as compared with Zr_Ni-**scu**-MOF-1, which is also lower from the expected value from the crystal structure.[39] The fact that FDM-182 was activated under very mild conditions using supercritical $CO_2$ while Zr_Ni-**scu**-MOF-1 by solvent exchange, suggest that our activation procedure is also successful and the observed reduced porosities in both cases could be associated with a slight pore contraction upon solvent removal. This proposition is supported by the pore size distribution (PSD) analysis. Accordingly, the PSD curves calculated using Non-Local Density Functional Theory (NLDFT) after a successful fitting of the Ar adsorption isotherm data using a suitable NLDFT kernel (cylindrical pores), revealing two main peaks centered at 5.4 and 8.7 Å for both Zr- and Hf-based solids (Figure 2b). The larger pore size is associated with the size of the 1D channels and is lower compared to the geometric value (9.2 Å) obtained by the Pore Analyzer tool, consistent with the observed reduced experimental pore volume. This is also the case for FDM-182, were the main PSD peak is centered at 8.5 Å, lower that the geometrically obtained value of 9.6 Å.[39] To gain further insight, we recorded the PXRD pattern of the activated Zr_Ni-**scu**-MOF-1, which shows some broadening of the Bragg peaks compared to that of the as-made solid (Figure S9). This suggests reduced long-range periodicity, likely due to framework deformation upon solvent removal, resulting in a smaller pore size and, in turn, lower porosity.

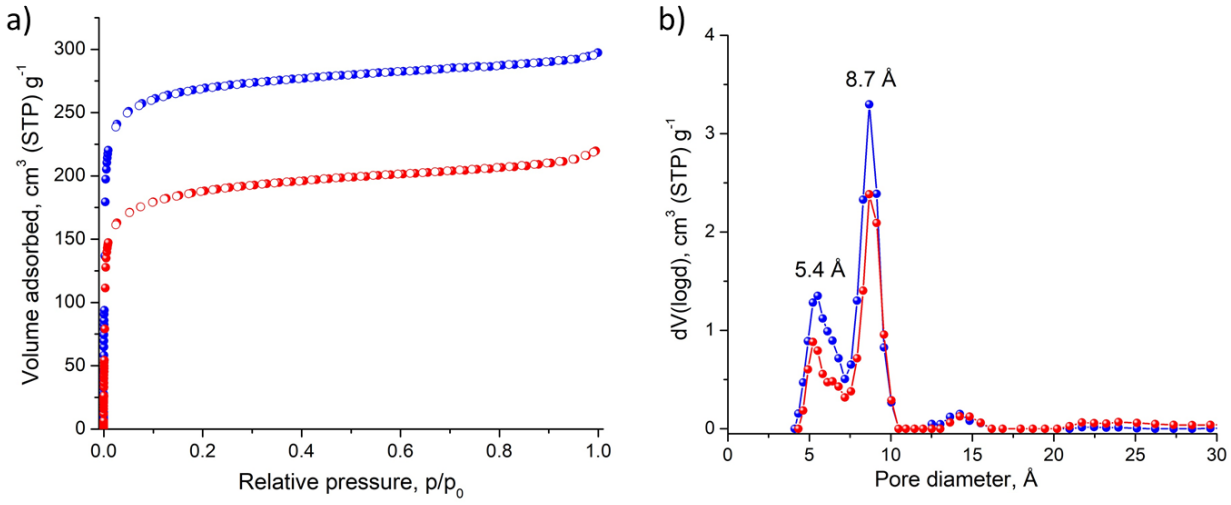


**Figure 2.** a) Argon sorption isotherms recorded at 87 K for Zr_Ni-**scu**-MOF-1 (blue) and Hf_Ni-**scu**-MOF-1 (red) solids. b) Pore size distribution curves obtained by NLDFT.

The strong synergism, emerging from the close proximity of the different metal clusters and the highly polar pore environment, originating from the metallo-ligand containing non-coordinated N atoms and $Cl^-$anions on the axial positions of the octahedral $Ni^{2+}$ complex, pointing to the

10.1002/chem.202501049

interior of the pore, prompted us to investigate the Xe/Kr separation properties by taking advantage of the higher polarizability of Xe over Kr. Accordingly, Xe and Kr adsorption isotherms were recorded at 273 K and 298 K up to 1 bar for both analogues. Notably, a relatively steep uptake of Xe at low pressures was revealed, compared to an almost linear increase in Kr uptake with increasing pressure. For Zr_Ni-**scu**-MOF-1, a high Xe uptake is recorded, reaching 73.6 $cm^3$ $g^{-1}$ (3.28 mmol $g^{-1}$) and 41.4 $cm^3$ $g^{-1}$ (1.85 mmol $g^{-1}$) at 273 K and 298 K respectively, at 1 bar, while the corresponding values for Kr are significantly reduced, reaching 28.3 $cm^3$ $g^{-1}$ (1.26 mmol $g^{-1}$)/11.8 $cm^3$ $g^{-1}$ (0.53 mmol $g^{-1}$) at 273 K/298 K and 1 bar (Figures 3a). From these isotherms, the calculated isosteric heat of adsorption at close to zero coverage ($Q_{st}^0$) is 26.4 kJ $mol^{-1}$ and 26.0 kJ $mol^{-1}$ for Xe and Kr respectively (Figures S17 and S19). Notably, the $Q_{st}^0$ value for Xe is comparable to that of MOFs possessing open metal sites and is well placed within the optimal range (17.5–35 kJ $mol^{-1}$) for efficient Xe/Kr separation and regeneration processes.[50-51] As function of the Xe uptake, the $Q_{st}$ values drop slightly reaching 23.8 kJ $mol^{-1}$ at 1 bar indicating a relatively uniform pore environment (Figure S17). For comparison purposes with the literature data, we calculated the IAST Xe/Kr selectivity for a 20/80 molar mixture at 298 K and the obtained value is 8.2 at low coverage (Figures 3c, S24, S25) which is higher compared to reported MOFs with a similar pore size and comparable to some of the best performing materials, as summarized in review articles.[50-51] It is note that in MOFs, an enhanced Xe/Kr selectivity is achieved with the presence of open metal sites (OMS) and/or ultramicroporous cavities (<7 Å), as for example in the cases of Cu-MOF-303 (8.2) and Ag-MOF-303 (10.4)[52], Mg-MOF-74 (7.5)[53], Zr-fum (8.2)[54], UTSA-74 (8.4)[55] and $Zn(ox)_{0.5}(trz)$ (10.2)[56], reported for a 20/80 mixture at 298 K. Taking in account that Zr_Ni-**scu**-MOF-1 does not contain OMS and displays a borderline ultramicroporosity (the PSD main peak is centered at 8.7 Å), the observed Xe/Kr selectivity is impressive and associated to the polar pore environment of the MOF. In the case of Hf_Ni-**scu**-MOF-1, the Xe/Kr at 298 K is 7.2 at low coverage and drops slightly to 6.3 at higher uptake (Figures 3c, S26, S27). In addition, a lower Xe and Kr gravimetric uptake is observed at 273K/298K and 1 bar, reaching 36/23.9 $cm^3$ $g^{-1}$ and 10.5/6.8 $cm^3$ $g^{-1}$ respectively, which is due to the heavier framework in combination to the lower isosteric heat of adsorption as compared to Zr_Ni-**scu**-MOF-1 (Figures S17, S19, S21 and S23). It is important to note that the observed difference in the total pore volume (these values were obtained from the Argon isotherm taking the point at 0.99 $p/p_o$, where the pores are filled) between Zr- and Hf_Ni-**scu**-MOF-1 cannot be directly compared with the differences in the Xe and Kr uptake, because in the latter cases the measurements were conducted well above the boiling point of these gases and at pressures up to 1 bar, only a fraction of the pore surface is covered. At these conditions, the pore size—linked to the degree of overlapping adsorption potentials—and specific gas–framework interactions, play a crucial role. Indeed, the calculated higher isosteric heat of adsorption for both Xe and Kr in Zr_Ni-**scu**-MOF-1 as compared to Hf_Ni-**scu**-MOF-1 are consistent with the observed differences in the corresponding uptake values.

10.1002/chem.202501049

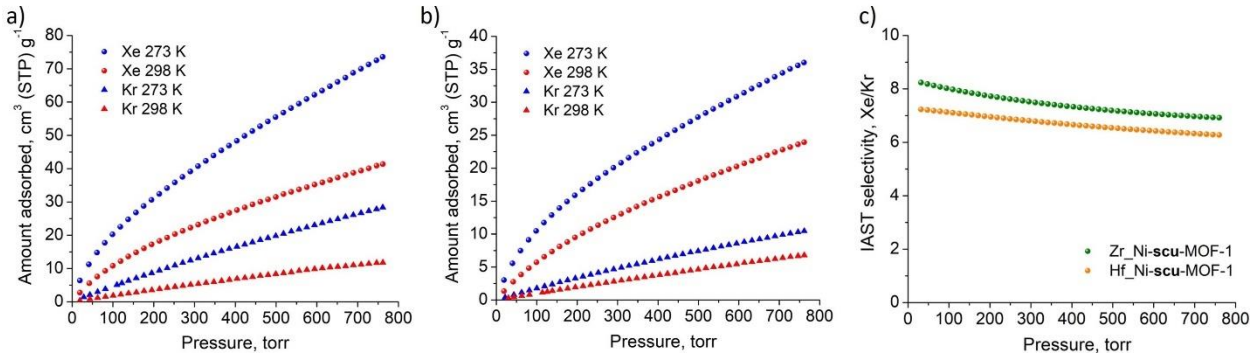


**Figure 3.** Xe and Kr adsorption isotherms of Zr_Ni-**scu**-MOF-1 (a) and Hf_Ni-**scu**-MOF-1 (b) at 273 K and 298 K up to 1 bar. c) IAST selectivity for a 20:80 Xe/Kr molar mixture at 298 K.

Encouraged by the polar pore environment of these MOFs, we also studied the $CO_2$ and $CH_4$ sorption properties and evaluated the $CO_2/CH_4$ selectivity which is important for numerous applications. Accordingly, sorption measurements at different temperatures and pressure up to 1 bar were performed (Figure 4). For Zr_Ni-**scu**-MOF-1, a high $CO_2$ uptake is observed that reaches 96.0 $cm^3 g^{-1}$ and 53.3 $cm^3 g^{-1}$ at 273 K and 298 K respectively, at 1 bar (Figure 4a). Notably, the $CO_2$ uptake at 298 K is significantly higher compare to FDM-182 (~31 $cm^3 g^{-1}$) under the same conditions,[39] representing a remarkable 72% increase. Although it has been reported that Ni-based MOFs shows an enhanced $CO_2$ uptake as compared to their Co-analogues, as in the case of Ni-MOF-74 and Co-MOF-74, where a 40% increase is reported at low pressure,[57] the observed difference between Zr_Ni-**scu**-MOF-1 and FDM-182 (Zr_Co-analogue) is not clear and its origin is currently under investigation.

In contrast to $CO_2$, the $CH_4$ sorption uptake in Zr_Ni-**scu**-MOF-1 is significantly lower, reaching 27.9/11.4 $cm^3 g^{-1}$ at 273K/298K at 1 bar, consistent with the lower $Q_{st}$ at low coverage, which was found to be 24.6 kJ $mol^{-1}$ while for $CO_2$ is 27.6 kJ $mol^{-1}$ (Figures 4a, S28-S31). In the case of Hf_Ni-**scu**-MOF-1, the total gravimetric uptake for $CO_2$ and $CH_4$ is lower compared to the Zr-analogue due to the heavier framework, reaching 55.9/30.4 $cm^3 g^{-1}$ and 14.3/6.5 $cm^3 g^{-1}$ at 273K/298K, respectively (Figures 4b), while the corresponding $Q_{st}$ values at low coverage are 25.8 and 23.7 kJ $mol^{-1}$ (Figures S32-S35). To evaluate the potential $CO_2/CH_4$ separation properties and for comparison purposes with literature data, we calculated the IAST

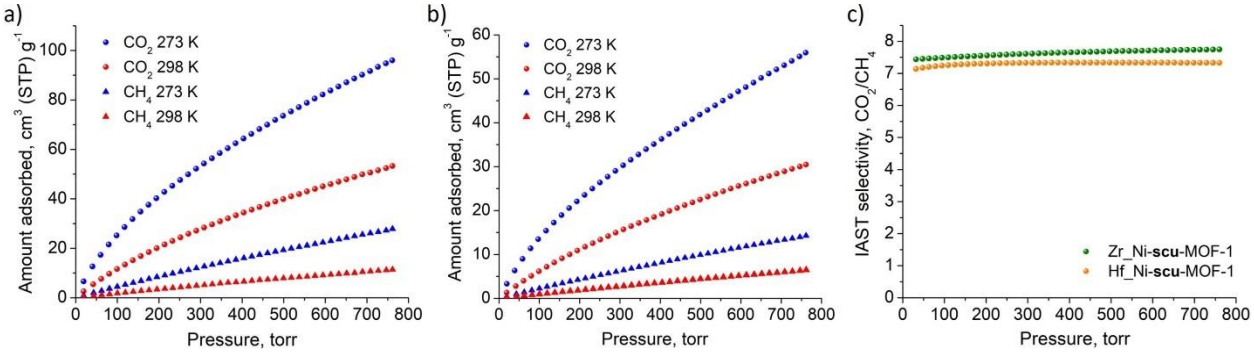


**Figure 4.** $CO_2$ and $CH_4$ adsorption isotherms of Zr_Ni-**scu**-MOF-1 (a) and Hf_Ni-**scu**-MOF-1 (b) at 273 K and 298 K up to 1 bar. c) IAST selectivity for a 5:95 $CO_2/CH_4$ molar mixture at 298 K.

selectivity for two representative molar mixtures, 5:95 and 50:50 at 298 K (Figures S36-S39). At low coverage the obtained value for a 5:95 mixture is 7.4 and 7.1 for Zr_Ni-**scu**-MOF-1 and Hf_Ni-**scu**-MOF-1 respectively and remains almost constant as a function of surface coverage (Figure 4c). Although these are moderate values, they compare very well with MOFs containing polar groups such as the sulfone functionalized Zr-UiO-67 (6.8) and Zr-flu-$SO_2$ (9.0) under the same conditions.[13, 58] Very similar values, 7.5 and 7.2 were obtained for a 50:50 molar mixture for the Zr_Ni-**scu**-MOF-1 and Hf_Ni-**scu**-MOF-1 at 298 K (Figure S40), which are very close to the reported value for FDM-182 (Zr_Co analogue), under the same conditions. The observed nearly constant $CO_2/CH_4$ IAST selectivity for the different gas phase compositions is not unusual and has been reported in the MOF literature, for example for ZJNU-40a[59], NOTT-101[59], and dia-7i-1-Co.[60]

## CONCLUSIONS

In conclusion, we report the direct synthesis of two isostructural bimetallic Zr/Hf-Ni M'MOFs, by the judicious implementation of Hard-Soft Chemistry. For our purpose, a dual functionality pyrazole-carboxylic acid ligand was selected and by fine control over the reaction conditions, a 4-connected non-planar $[Ni(HPyC)_4Cl_2]^{4-}$ metallo-ligand based was formed in-situ and bridges 8-connected $M_6O_4(OH)_4(\text{-}COO)_8$ (M: $Zr^{4+}$, $Hf^{4+}$) clusters, resulting in a three dimensional open framework displaying the (4, 8)-c **scu**-a topology. The non-planar $[Ni(HPyC)_4Cl_2]^{4-}$ metallo-ligand results in a polygonal shaped 1D cavities of the **scu** network and the formation of a polar pore environment that was found accessible and fully characterized by detailed Ar sorption measurements at 87 K. Due to the unique structural features, the Xe/Kr and $CO_2/CH_4$ separation properties were studied in both Zr-Ni-**scu**-MOF-1 and Hf_Ni-**scu**-MOF-1. Accordingly, the IAST selectivity calculated for a 20:80 Xe/Kr molar mixture is 8.2 and 7.1 at 298K for the Zr_Ni-**scu**-MOF-1 and Hf_Ni-**scu**-MOF-1, respectively, which is higher compared to reported MOFs with a similar pore size and comparable to some of the best performing materials. The corresponding

values for a 5:95 $CO_2/CH_4$ molar mixture are 7.5 and 7.2, which compare very well with MOFs containing polar groups.

The successful synthesis of M_Ni-**scu**-MOF-1 (M: $Zr^{4+}$, $Hf^{4+}$) demonstrates that under controlled reaction conditions, the HSAB principle can be effectively utilized for the development of heterometallic MOFs based on suitable multifunctional ligands. Accordingly, we envisioned a reticular chemistry approach for the design and synthesis of novel heterometallic MOFs based on edge-transitive nets other than **scu**, greatly expanding the family of these important solids.

**ACKNOWLEDGEMENTS**

This study was carried out within the framework of the National Recovery and Resilience Plan Greece 2.0 (Award Number TAEDR-0535821), funded by the European Union – NextGenerationEU.

**CONFLICT OF INTEREST**

The authors declare no conflict of interest.

## REFERENCES

[1] M. Ding, R. W. Flaig, H.-L. Jiang, O. M. Yaghi, *Chem. Soc. Rev.* **2019**, *48*, 2783-2828.
[2] H. Furukawa, K. E. Cordova, M. O'Keeffe, O. M. Yaghi, *Science* **2013**, *341*, 1230444.
[3] H. Furukawa, F. Gándara, Y.-B. Zhang, J. Jiang, W. L. Queen, M. R. Hudson, O. M. Yaghi, *J. Am. Chem. Soc.* **2014**, *136*, 4369-4381.
[4] H. N. García, S., *Metal-Organic Frameworks (MOFs): Applications in Separations and Catalysis. Wiley-VCH 2018.*
[5] S. K. Ghosh, *Metal-Organic Frameworks (MOFs) for Environmental Applications. Elsevier 2019.* .
[6] C. H. Hendon, A. J. Rieth, M. D. Korzyński, M. Dincă, *ACS Cent. Sci.* **2017**, *3*, 554-563.
[7] S. Kaskel, *The Chemistry of Metal-Organic Frameworks. Wiley-VCH* **2016**.
[8] J. D. Wuest, *Nat. Commun* **2020**, *11*, 4652.
[9] M. Eddaoudi, D. B. Moler, H. Li, B. Chen, T. M. Reineke, M. O'Keeffe, O. M. Yaghi, *Acc. Chem. Res.* **2001**, *34*, 319-330.
[10] D.-X. Xue, A. Cadiau, Ł. J. Weseliński, H. Jiang, P. M. Bhatt, A. Shkurenko, L. Wojtas, C. Zhijie, Y. Belmabkhout, K. Adil, M. Eddaoudi, *Chem. Comm.* **2018**, *54*, 6404-6407.
[11] Z. Chen, S. L. Hanna, L. R. Redfern, D. Alezi, T. Islamoglu, O. K. Farha, *Coord. Chem. Rev.* **2019**, *386*, 32-49.
[12] D. Alezi, I. Spanopoulos, C. Tsangarakis, A. Shkurenko, K. Adil, Y. Belmabkhout, M. O'Keeffe, M. Eddaoudi, P. N. Trikalitis, *J. Am. Chem. Soc.* **2016**, *138*, 12767-12770.
[13] G. K. Angeli, D. Batzavali, K. Mavronasou, C. Tsangarakis, T. Stuerzer, H. Ott, P. N. Trikalitis, *J. Am. Chem. Soc.* **2020**, *142*, 15986-15994.
[14] M. J. Kalmutzki, N. Hanikel, O. M. Yaghi, *Sci. Adv.*, *4*, eaat9180.
[15] A. Dhakshinamoorthy, Z. Li, S. Yang, H. Garcia, *Chem. Soc. Rev.* **2024**, *53*, 3002-3035.
[16] V. Fernandes de Almeida, S. Navalón, A. Dhakshinamoorthy, H. Garcia, *Angew. Chem. Int. Ed.* **2025**, *64*, e202424537.
[17] H. Furukawa, U. Müller, O. M. Yaghi, *Angew. Chem. Int. Ed.* **2015**, *54*, 3417-3430.

[18] M. Viciano-Chumillas, X. Liu, A. Leyva-Pérez, D. Armentano, J. Ferrando-Soria, E. Pardo, *Coord. Chem. Rev.* **2022**, *451*, 214273.

[19] M. Y. Masoomi, A. Morsali, A. Dhakshinamoorthy, H. Garcia, *Angew. Chem. Int. Ed.* **2019**, *58*, 15188-15205.

[20] J. Pei, X.-W. Gu, C.-C. Liang, B. Chen, B. Li, G. Qian, *J. Am. Chem. Soc.* **2022**, *144*, 3200-3209.

[21] P. Elumalai, H. Mamlouk, W. Yiming, L. Feng, S. Yuan, H.-C. Zhou, S. T. Madrahimov, *ACS Appl. Mater. Interfaces* **2018**, *10*, 41431-41438.

[22] M. Dincă, J. R. Long, *J. Am. Chem. Soc.* **2007**, *129*, 11172-11176.

[23] F. Song, C. Wang, J. M. Falkowski, L. Ma, W. Lin, *J. Am. Chem. Soc.* **2010**, *132*, 15390-15398.

[24] C.-D. Wu, A. Hu, L. Zhang, W. Lin, *J. Am. Chem. Soc.* **2005**, *127*, 8940-8941.

[25] C.-D. Wu, W. Lin, *Angew. Chem. Int. Ed.* **2007**, *46*, 1075-1078.

[26] L. Ma, J. M. Falkowski, C. Abney, W. Lin, *Nat. Chem* **2010**, *2*, 838-846.

[27] B. Chen, X. Zhao, A. Putkham, K. Hong, E. B. Lobkovsky, E. J. Hurtado, A. J. Fletcher, K. M. Thomas, *J. Am. Chem. Soc.* **2008**, *130*, 6411-6423.

[28] S. Nayak, K. Harms, S. Dehnen, *Inorg. Chem.* **2011**, *50*, 2714-2716.

[29] P.-F. Shi, H.-C. Hu, Z.-Y. Zhang, G. Xiong, B. Zhao, *Chem. Comm.* **2015**, *51*, 3985-3988.

[30] I. Spanopoulos, I. Bratsos, C. Tampaxis, D. Vourloumis, E. Klontzas, G. E. Froudakis, G. Charalambopoulou, T. A. Steriotis, P. N. Trikalitis, *Chem. Comm.* **2016**, *52*, 10559-10562.

[31] E. Miguel-Casañ, M. D. Darawsheh, V. Fariña-Torres, I. J. Vitórica-Yrezábal, E. Andres-Garcia, M. Fañanás-Mastral, G. Mínguez Espallargas, *Chem. Sci.* **2023**, *14*, 179-185.

[32] I. Bratsos, C. Tampaxis, I. Spanopoulos, N. Demitri, G. Charalambopoulou, D. Vourloumis, T. A. Steriotis, P. N. Trikalitis, *Inorg. Chem.* **2018**, *57*, 7244-7251.

[33] A. Schoedel, A. J. Cairns, Y. Belmabkhout, L. Wojtas, M. Mohamed, Z. Zhang, D. M. Proserpio, M. Eddaoudi, M. J. Zaworotko, *Angew. Chem. Int. Ed.* **2013**, *52*, 2902-2905.

[34] J. Ferrando-Soria, P. Serra-Crespo, M. de Lange, J. Gascon, F. Kapteijn, M. Julve, J. Cano, F. Lloret, J. Pasán, C. Ruiz-Pérez, Y. Journaux, E. Pardo, *J. Am. Chem. Soc.* **2012**, *134*, 15301-15304.

[35] W. Gong, H. Arman, Z. Chen, Y. Xie, F. A. Son, H. Cui, X. Chen, Y. Shi, Y. Liu, B. Chen, O. K. Farha, Y. Cui, *J. Am. Chem. Soc.* **2021**, *143*, 657-663.

[36] S.-C. Xiang, Z. Zhang, C.-G. Zhao, K. Hong, X. Zhao, D.-R. Ding, M.-H. Xie, C.-D. Wu, M. C. Das, R. Gill, K. M. Thomas, B. Chen, *Nat. Commun.* **2011**, *2*, 204.

[37] M. E. Kosal, J.-H. Chou, S. R. Wilson, K. S. Suslick, *Nat. Mater.* **2002**, *1*, 118-121.

[38] P. F. Muldoon, C. Liu, C. C. Miller, S. B. Koby, A. Gamble Jarvi, T.-Y. Luo, S. Saxena, M. O'Keeffe, N. L. Rosi, *J. Am. Chem. Soc.* **2018**, *140*, 6194-6198.

[39] Y. Wu, H. Xu, X. Li, Y. Rao, S. Yuan, Y. Yan, Y.-B. Zhang, Q. Li, *Small* **2024**, *20*, 2402314.

[40] D. Feng, Z.-Y. Gu, J.-R. Li, H.-L. Jiang, Z. Wei, H.-C. Zhou, *Angew. Chem. Int. Ed.* **2012**, *51*, 10307-10310.

[41] J. Lyu, X. Zhang, K.-i. Otake, X. Wang, P. Li, Z. Li, Z. Chen, Y. Zhang, M. C. Wasson, Y. Yang, P. Bai, X. Guo, T. Islamoglu, O. K. Farha, *Chem. Sci.* **2019**, *10*, 1186-1192.

[42] M. Lammert, H. Reinsch, C. A. Murray, M. T. Wharmby, H. Terraschke, N. Stock, *Dalton Trans.* **2016**, *45*, 18822-18826.

[43] K. Wu, J. Zheng, Y.-L. Huang, D. Luo, Y. Y. Li, W. Lu, D. Li, *J. Mater. Chem. C* **2020**, *8*, 16974-16983.

[44] J. Pang, S. Yuan, D. Du, C. Lollar, L. Zhang, M. Wu, D. Yuan, H.-C. Zhou, M. Hong, *Angew. Chem. Int. Ed.* **2017**, *56*, 14622-14626.

[45] C. F. Macrae, I. Sovago, S. J. Cottrell, P. T. A. Galek, P. McCabe, E. Pidcock, M. Platings, G. P. Shields, J. S. Stevens, M. Towler, P. A. Wood, *J. Appl. Crystallogr.* **2020**, *53*, 226-235.

[46] A. Direm, M. Tursun, C. Parlak, N. Benali-Cherif, *J. Mol. Struct.* **2015**, *1093*, 208-218.

[47] C. W. Reimann, A. D. Mighell, F. A. Mauer, *Acta Crystallogr.* **1967**, *23*, 135-141.

[48] X.-J. Kong, T. He, A. A. Bezrukov, S. Darwish, G.-R. Si, Y.-Z. Zhang, W. Wu, Y. Wang, X. Li, N. Kumar, J.-R. Li, M. J. Zaworotko, *J. Am. Chem. Soc.* **2024**, *146*, 28320-28328.
[49] N. M. Padial, E. Quartapelle Procopio, C. Montoro, E. López, J. E. Oltra, V. Colombo, A. Maspero, N. Masciocchi, S. Galli, I. Senkovska, S. Kaskel, E. Barea, J. A. R. Navarro, *Angew. Chem. Int. Ed.* **2013**, *52*, 8290-8294.
[50] Y. Yang, C. Tu, L. Guo, L. Wang, F. Cheng, F. Luo, *Cell Rep. Phys. Sci.* **2023**, *4*, 101694.
[51] D. Banerjee, C. M. Simon, S. K. Elsaidi, M. Haranczyk, P. K. Thallapally, *Chem* **2018**, *4*, 466-494.
[52] H. Wang, Z. Shi, J. Yang, T. Sun, B. Rungtaweevoranit, H. Lyu, Y.-B. Zhang, O. M. Yaghi, *Angew. Chem. Int. Ed.* **2021**, *60*, 3417-3421.
[53] S. K. Ghose, Y. Li, A. Yakovenko, E. Dooryhee, L. Ehm, L. E. Ecker, A.-C. Dippel, G. J. Halder, D. M. Strachan, P. K. Thallapally, *J. Phys. Chem. Lett.* **2015**, *6*, 1790-1794.
[54] Z. Yan, Y. Gong, B. Chen, X. Wu, Q. liu, L. Cui, S. Xiong, S. Peng, *Sep. Purif. Technol.* **2020**, *239*, 116514.
[55] Y. Tao, Y. Fan, Z. Xu, X. Feng, R. Krishna, F. Luo, *Inorg. Chem.* **2020**, *59*, 11793-11800.
[56] L. Yu, S. Xiong, Y. Lin, L. Li, J. Peng, W. Liu, X. Huang, H. Wang, J. Li, *Inorg. Chem.* **2019**, *58*, 15025-15028.
[57] J. Liu, P. K. Thallapally, B. P. McGrail, D. R. Brown, J. Liu, *Chem. Soc. Rev.* **2012**, *41*, 2308-2322.
[58] P. Xydias, I. Spanopoulos, E. Klontzas, G. E. Froudakis, P. N. Trikalitis, *Inorg. Chem.* **2014**, *53*, 679-681.
[59] C. Song, Y. He, B. Li, Y. Ling, H. Wang, Y. Feng, R. Krishna, B. Chen, *Chem. Comm.* **2014**, *50*, 12105-12108.
[60] T. Pham, K. A. Forrest, B. Tudor, S. K. Elsaidi, M. H. Mohamed, K. McLaughlin, C. R. Cioce, M. J. Zaworotko, B. Space, *Langmuir* **2014**, *30*, 6454-6462.

10.1002/chem.202501049

**TABLE OF CONTENTS**

Successful implementation of the HSAB principle using a bifunctional pyrazole-carboxylic acid organic linker afforded in one pot synthesis heterometallic (Zr/Ni and Hf/Ni) MOFs with a polar pore environment, suitable for gas separation applications.